Histol Histopathol (2024) 39: 1457-1472

Histology and Histopathology
From Cell Biology to Tissue Engineering

ORIGINAL ARTICLE Open Access

"Vascular tuft sign" in neuroendocrine tumors of the pancreas

L. Díaz-Flores[1], R. Gutiérrez[1], M.P. García-Suárez[2], M. González-Gómez[1,3], J.L. Carrasco[1], J.F. Madrid[4] and L. Díaz-Flores Jr[5]

[1]Department of Basic Medical Sciences, Faculty of Medicine, University of La Laguna, [2]Department of Pathology, Hospiten® Hospitals, [3]Instituto de Tecnologías Biomédicas de Canarias, University of La Laguna, Tenerife, [4]Department of Cell Biology and Histology, School of Medicine, Regional Campus of International Excellence "Campus Mare Nostrum", IMIB-Arrixaca, University of Murcia, Murcia and [5]Department of Physical Medicine and Pharmacology, Faculty of Medicine, University of La Laguna, Tenerife, Spain

Summary. The often well-developed microvasculature in pancreatic neuroendocrine tumors (PanNETs) has been studied from different perspectives. However, some detailed structural findings have received less attention. Our objective is to study an overlooked event in PanNETs: "enclosed vascular tufts" (EVTs). For this purpose, 39 cases of PanNETs were examined with conventional (including serial sections) and immunochemistry procedures. In typical EVTs, the results show: 1) an insulated terminal vascular area, with a globular (glomeruloid) aspect, formed by a cluster of coiled microvessels, presenting CD31-, CD34-positive endothelial cells, αSMA-positive pericytes, and perivascular CD34-positive stromal cells/telocytes, separated by a pseudoglandular space from the surrounding trabeculae of tumor neuroendocrine cells; and 2) a pedicle joining the insulated terminal vascular area, with connective tissue tracts around the enclosing tumor trabeculae. EVTs predominate in the trabecular and nested gyriform pattern of PanNETs, with tumor trabeculae that follow a ribbon coil (winding ribbon pattern) around small vessels, which acquire a tufted image. In EVTs, secondary modifications may occur (fibrosis, hyalinization, myxoid changes, and calcification), coinciding or not with those of the connective tracts. In conclusion, the typical characteristics of unnoticed EVTs allow them to be considered as a morphological sign of PanNETs (a vascular tuft sign). Further in-depth studies are required, mainly to assess the molecular pathways that participate in vascular tuft formation and its pathophysiological implications.

Corresponding Author: Lucio Díaz-Flores, Departamento de Ciencias Médicas Básicas, Facultad de Medicina, Universidad de La Laguna, Tenerife, Spain. e-mail: kayto54@gmail.com
www.hh.um.es. DOI: 10.14670/HH-18-787

Key words: Pancreas, Neuroendocrine tumors, CD34-positive stromal cells/telocytes, αSMA-positive myofibroblasts, Vascular tuft sign

Introduction

The incidence of neuroendocrine neoplasms, including those of the pancreas (PanNENs), has increased considerably in recent decades mainly due to improvements in diagnostic methods, especially in cases with an indolent asymptomatic clinical course, and screening campaigns (Falconi et al., 2012; Dasari et al., 2017; Xu et al., 2021; Rossi and Massironi, 2022). WHO classifications of neuroendocrine neoplasms, based on different parameters including morphologic characteristics, mitotic activity, Ki-67 proliferative index, and other immunohistochemical profiles, have improved since 2010 (Klimstra et al., 2010; Kim et al., 2017; Yang et al., 2020; Rindi et al., 2022). Thus, PanNENs are classified as Grade 1, 2, or 3 pancreatic neuroendocrine tumors (G1, G2, G3 PanNETs) and Grade 3 pancreatic neuroendocrine carcinomas (G3 PanNECs). The classic histological patterns of PanNETs - including solid, nested, organoid, gyriform or winding ribbon, and glandular - have also been refined in different classifications, mainly to give functional or prognostic meaning (Kasajima and Klöppel, 2020; Xue et al., 2020). For functional meaning, classificatory morphologic patterns include trabecular and solid tumors. Those with a trabecular pattern may occur with amyloid deposition (secreting insulin) or with a reticular-trabecular image and cystic changes (secreting glucagon), whereas those with a solid pattern and paraganglioma-like features usually secrete somatostatin (Garbrecht et al., 2008; McCall et al., 2012; Konukiewitz et al., 2017, 2020; Kasajima and Klöppel, 2020). In the prognostic meaning, the classificatory

morphologic patterns include a) "metabolically active cells" presenting diffuse growth, nucleoli, and abundant cytoplasm, with an oncocytic, lipid-rich, plasmacytoid, or hepatoid aspect (more aggressive), b) paraganglioid or organoid characteristics and possible degenerative changes, or nested growth (less aggressive), and c) a pseudoglandular, sclerotic, peliotic, or mammary tubulolobular aspect (undetermined) (Xue et al., 2020).

The PanNET microenvironment has been considered in several studies that have focused on cancer-associated fibroblasts, vessels, inflammatory cells, extracellular matrix, and fibrosis (Laskaratos et al., 2017; Cives et al., 2019; Takkenkamp et al., 2020; Chmiel et al., 2023; Lai et al., 2024). Microvascular density changes, mainly those associated with fibrosis, angiogenic phenomena, and tumoral vessel invasion, were the major objectives of studies on PanNET vessels (Bok et al., 1984; Couvelard et al., 2005; Schmid et al., 2005; Norton et al., 2011; Balachandran et al., 2012; Carrasco et al., 2017; Addeo et al., 2019; Lafaro and Melstrom, 2019; Liu and Polydorides, 2020; Lauricella et al., 2022). However, detailed structural events of PanNET microvasculature have received less attention. In a histological study of PanNET microvasculature (unpublished observations), we identified an overlooked morphologic event: enclosed vascular tufts (EVTs). The structural description of this finding is of interest to lay the basis to support subsequent pathophysiological investigations.

Given the above, this study aims to examine an overlooked event (EVTs) in the microvasculature of PanNETs as a morphologic sign: the "vascular tuft sign" in these neuroendocrine tumors. To that end, the following aspects were considered: a) typical characteristics of EVTs with conventional techniques (hematoxylin and eosin staining) and immunochemistry procedures, b) secondary changes, c) incidence depending on the PanNET morphological pattern, and d) the relationship with other components of the stroma and the association with other structures. For this purpose, 39 cases of PanNETs were studied with conventional histological techniques and immunohistochemical procedures.

Materials and methods

Human tissue samples

The Histology and Anatomical Pathology archives of the Departments of Basic Medical Sciences of La Laguna University, University Hospital, and Eurofins® Megalab–Hospiten Hospitals of the Canary Islands were searched for cases of PanNETs. Paraffin blocks obtained from surgical specimens from 39 Caucasian patients (22 males and 17 females), with ages ranging from 41 to 86 years, were used. The samples were studied by conventional histological techniques and immunochemistry procedures. Ethical approval for this study was obtained from the Ethics Committee of La Laguna University (Comité de Ética de la Investigación y de Bienestar Animal, CEIBA 2024-3418), including the dissociation of the samples from any information that could identify the patient. The authors, therefore, had no access to identifiable patient information.

Light microscopy

The specimens were fixed in a buffered, neutral 4% formaldehyde solution, embedded in paraffin, and cut into 3-µm-thick sections. Serial sections were also obtained in demonstrative blocks. The sections were deparaffinized, hydrated, and underwent hematoxylin and eosin, and trichrome staining (Roche, Basel, Switzerland. Ref. 6521908001).

Immunohistochemistry

Immunohistochemistry (automated and manual procedures) were carried out as described elsewhere (Díaz-Flores, et al., 2018, 2023). For the automated immunohistochemistry procedure, sections were incubated with the following primary antibodies from Leica Biosystems (Newcastle, UK) for CD34 (Bond™ Ref PA0212), CD31 (Bond™ Ref PA0250), αSMA (Bond™ PA0943), Vimentin (Bond™ PA0640), Desmin (Bond™ PA0032), CD10 (Bond™ Ref PA0270), CD56 (Bond™ Ref PA0191), EMA (Bond™ PA0015), Calponin (Bond™ PA0416), Protein S100 (Bond™ PA0031), Chromogranin (Bond™ PA 0515), and Synaptophysin (Bond™ PAO299). The nonautomated procedure used rabbit polyclonal anti-CD34 (1/100 dilution, code no. A13929, ABclonal, Woburn, MA, USA) and mouse monoclonal anti-αSMA (1/100 dilution, code no. ABK1-A8914, Abyntek Biopharma, Zamudio, Spain). The immunoreaction was developed in a solution of diaminobenzidine, and the sections were then briefly counterstained with hematoxylin, dehydrated in an ethanol series, cleared in xylene, and mounted in Eukitt®. Positive and negative controls were used.

Results

General characteristics of PanNETs

All PanNETs were well-differentiated with a trabecular or solid pattern. Cases with a predominant trabecular pattern (n: 25) adopted a gyriform (winding ribbon, cribriform, or pseudoglandular) or cordonal (linear or undulate) morphology. Although there was a predominant pattern, areas with morphological characteristics of other patterns may be intermingled. Cases with a solid pattern (n: 14) were arranged diffusely or in nests/islets. The PanNET neuroendocrine cells generally showed oval or round nuclei, with a salt-and-pepper aspect of the chromatin and eosinophilic, pale, or amphophilic cytoplasm. The number of mitoses was less than 20/2 mm^2 and the Ki67 index was less

than 20%. Psammoma bodies were present in four cases and hyaline bodies in two; peliosis was seen in two cases. Tumor necrosis was not observed. The stroma showed connective tracts of variable amplitude. Cases with intense fibrosis (n: 5), hyalinization (n: 3), and calcification (n: 2) were seen. Perineural and vascular (predominantly in veins) invasion occurred in three and five cases, respectively.

Typical characteristics of EVTs in PanNETs

The typical histological appearance of the EVTs observed with conventional techniques (hematoxylin and eosin staining) was that of highly cellular, often globular, structures surrounded by tumor neuroendocrine cells, from which they were frequently separated by a pseudoglandular space (Fig. 1). When EVTs were globular, they showed a glomeruloid aspect (Fig. 1). Immunohistochemical procedures revealed that the neuroendocrine tumor cells were positive for synaptophysin, chromogranin, and CD56, whereas the cells in the tuft structures were negative for these markers (Fig. 2). When the surrounding tumoral cells were arranged in a single layer and totally or partially delimited by stromal tracts, the appearance of glands with intraluminal globular structures was more marked.

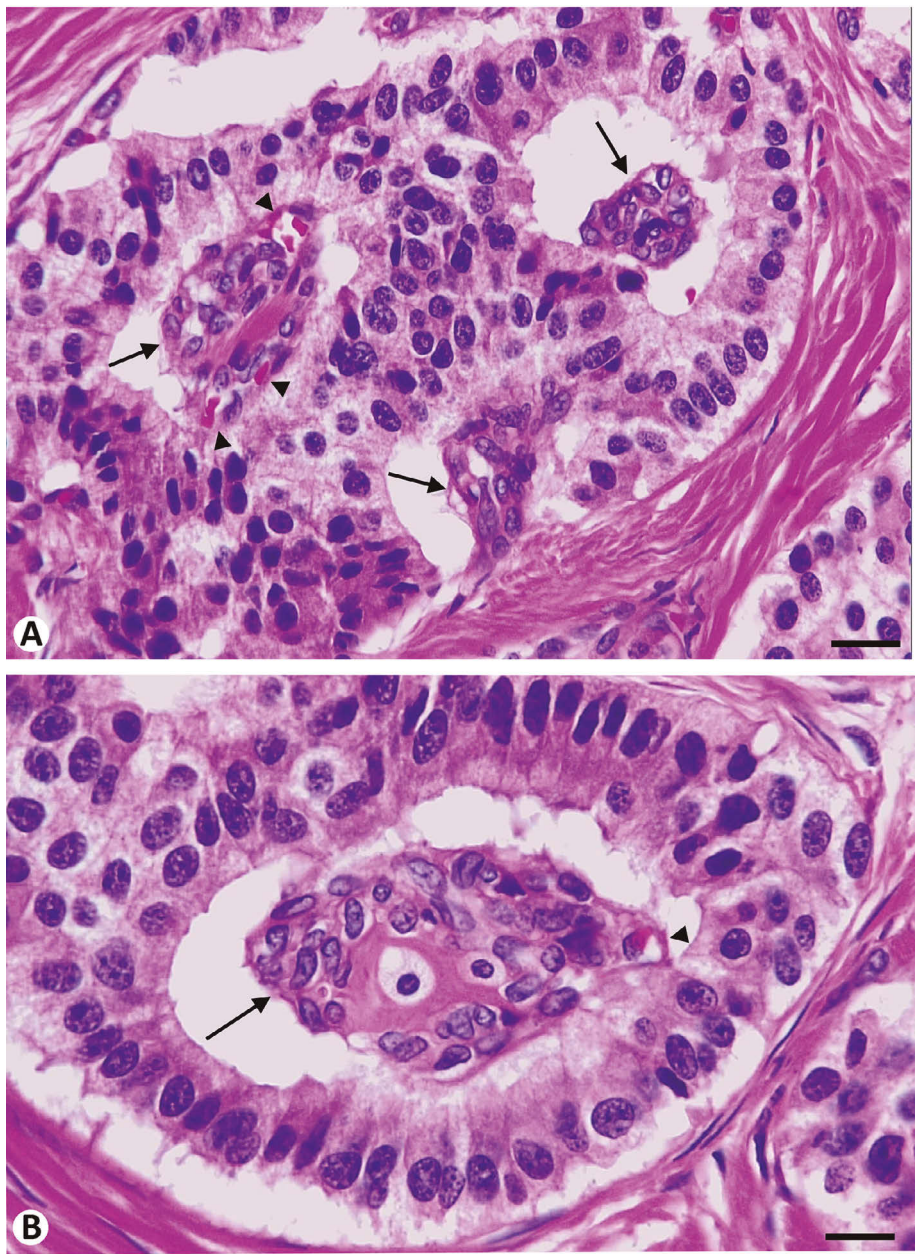

Fig. 1. A, B. Typical characteristics of EVTs (arrows), which show high cellularity and are surrounded by neuroendocrine tumor cells. Note the globular or glomeruloid appearance of EVTs and the separation space between them and the surrounding neuroendocrine cells, in a gyriform-pseudoglandular arrangement. Some minute blood vessels are identified by the presence of red blood cells in their lumens (arrowhead). Hematoxylin and eosin staining. Scale bars: A, 15 µm; B, 10 µm.

The intraluminal EVTs in the pseudoglandular structures could be observed connecting with the connective tracts by pedicles of variable width, however, they were generally thin (Fig. 3). Occasionally, EVTs were branched (Fig. 4A) or multiple and interconnected (Fig. 4B). The cells of the EVTs mainly differed from the

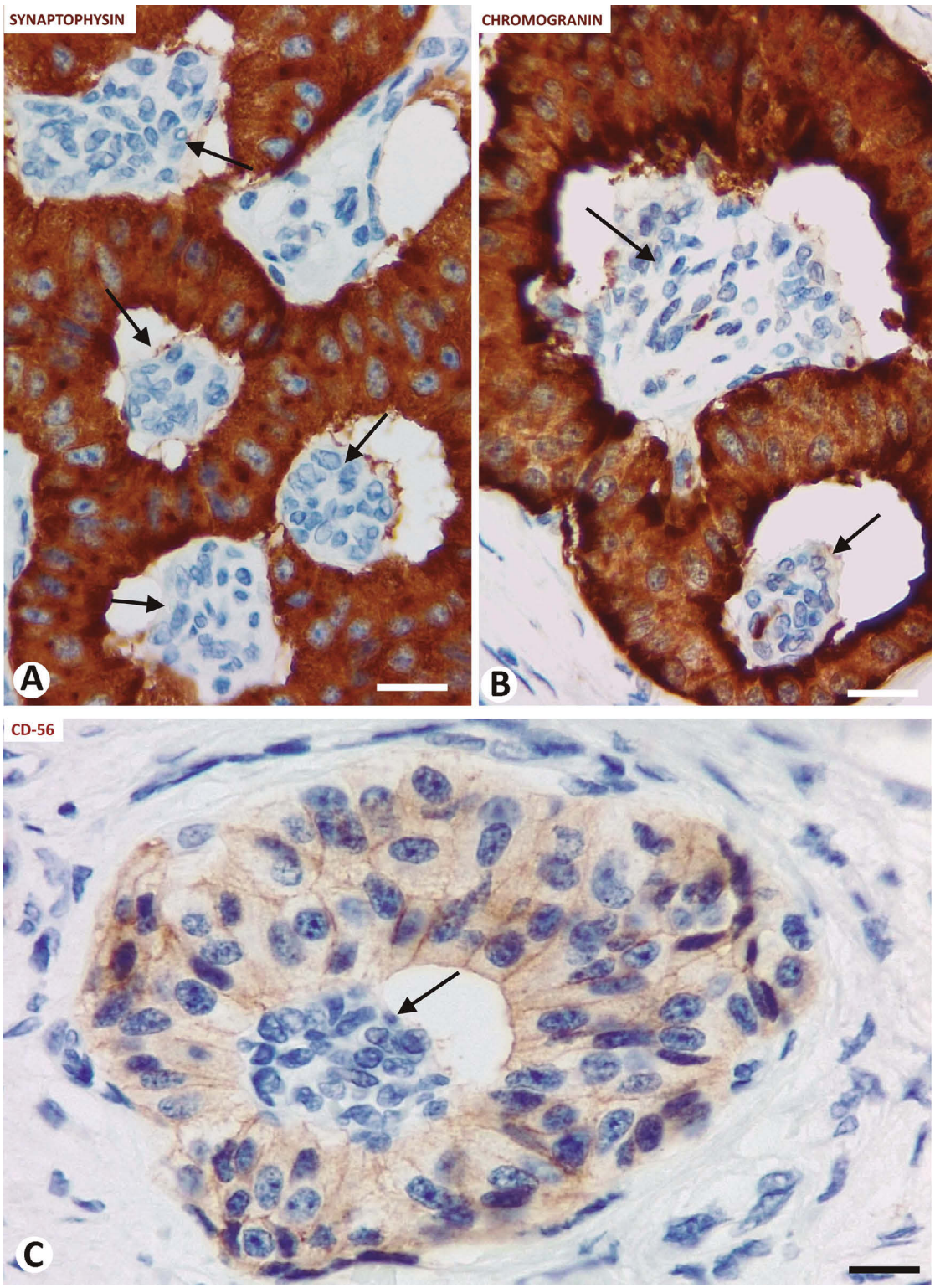

Fig. 2. Positivity for neuroendocrine cell markers is observed in tumor cells, although these markers are not expressed in EVT cells (arrows). **A-C.** Immunochemistry for synaptophysin **(A)**, chromogranin **(B)**, and CD56 **(C)**. Hematoxylin counterstain. Scale bars: A, B, 20 µm; C, 15 µm.

surrounding tumor neuroendocrine cells as their nuclei were smaller, less stained, and without the salt-and-pepper aspect of the neuroendocrine tumor cells (Fig. 5A). Clusters of coiled, minute blood vessels were an important component of the EVTs (vascular EVTs in the lumen of pseudoglandular structures: vascular tuft sign) (Figs. 1, 3, 5B). Many minute vessels showed small or virtual lumens, which were difficult to identify with conventional techniques (e.g., hematoxylin and eosin staining), and the EVTs had the aforementioned highly cellular aspect. Nevertheless, the presence of one or several intraluminal red blood cells in some EVT vessels facilitated vessel identification (Figs. 1, 3, 5B). Stromal cells and extracellular matrix components were also observed in EVTs.

In EVTs, endothelial cells of the blood vessels were positive for CD34 (Fig. 6A,B) and CD31 (Fig. 6C); αSMA expression was observed in blood vessel mural cells (mainly pericytes and occasionally vascular smooth muscle cells) (Fig. 7A). Positivity for CD34 was also evident in perivascular stromal cells of the EVTs (CD34+ stromal cells/telocytes). Endothelial, mural, and stromal cells were positive for vimentin (Fig. 7B) and negative for desmin, CD10, EMA, calponin, protein

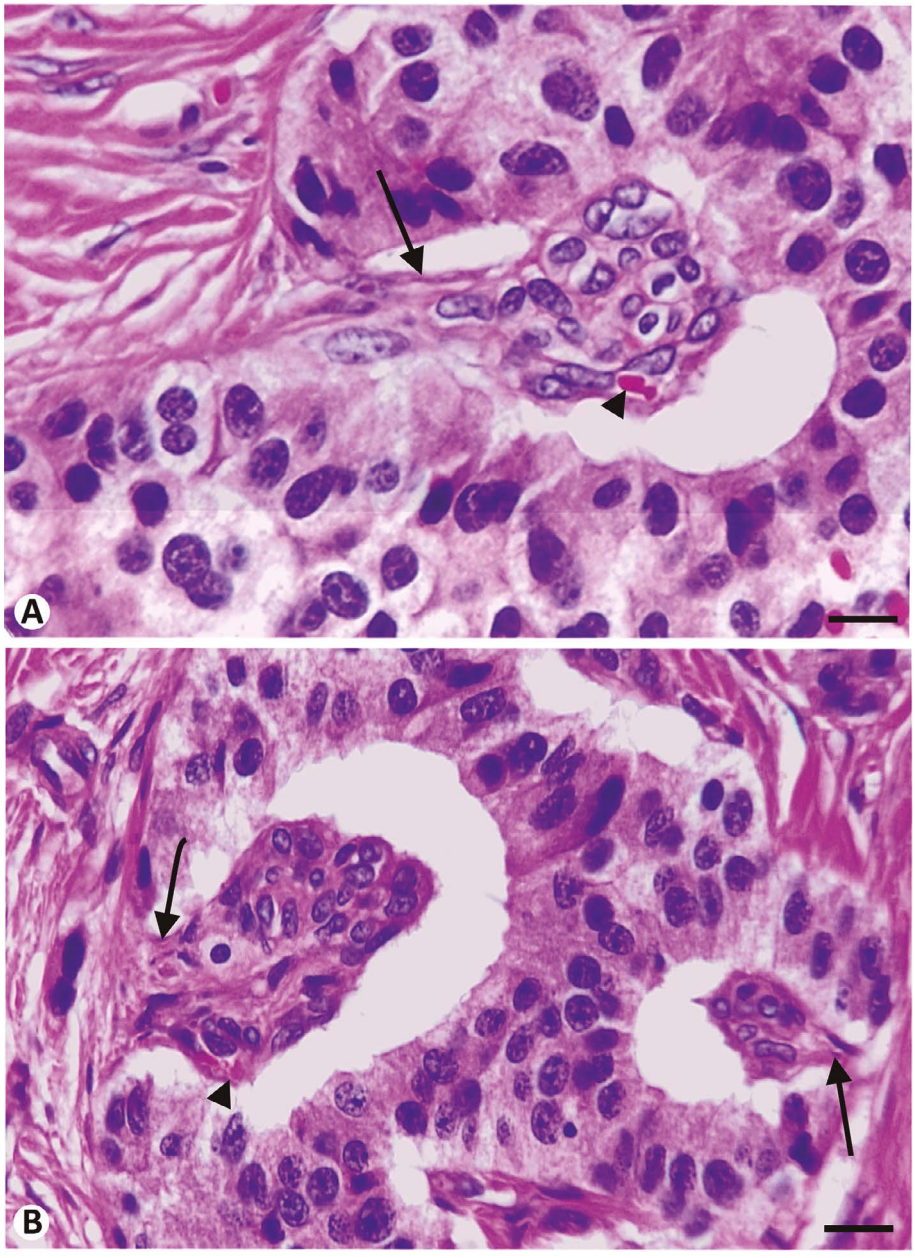

Fig. 3. A, B. EVT pedicles (arrows) of different lengths and thicknesses are observed in the EVTs within the gyriform-pseudoglandular structures. Note that the VT pedicles connect the EVTs with the connective tracts that surround the gyriform structures. Some minute blood vessels with red blood cells are observed (arrowheads). Hematoxylin and eosin staining. Scale bars: A, 10 µm; B, 15 µm.

S100, chromogranin, synaptophysin, and CD56.

Secondary changes in EVTs

Some EVTs showed secondary changes according to the case and even within an area of the same case. The main modifications of EVTs were total or partial fibrosis and/or hyalinization, edematous and myxoid changes, as well as the presence of inflammatory infiltrates (Fig. 8). The hyalinization of EVTs occurred predominantly in their central area, in which the hyaline component increases tuft size and pushes the vascular and stromal cells toward the tuft periphery, forming a thin strip (Fig. 8A). Foci of calcification could occur in the hyaline component (Fig. 8B). Although similar modifications were also present in the connective tracts surrounding the gyriform/winding ribbon structures, whether they were coincident or not depended on the tumor region (Fig. 8C,D) and occurred relatively frequently in the connective tracts, whereas the EVTs were unmodified (Fig. 8D). The hyaline exhibited differences with the so-called hyaline bodies observed in three of our cases. The inflammatory infiltrate was mainly formed by mononuclear cells (Fig. 8E).

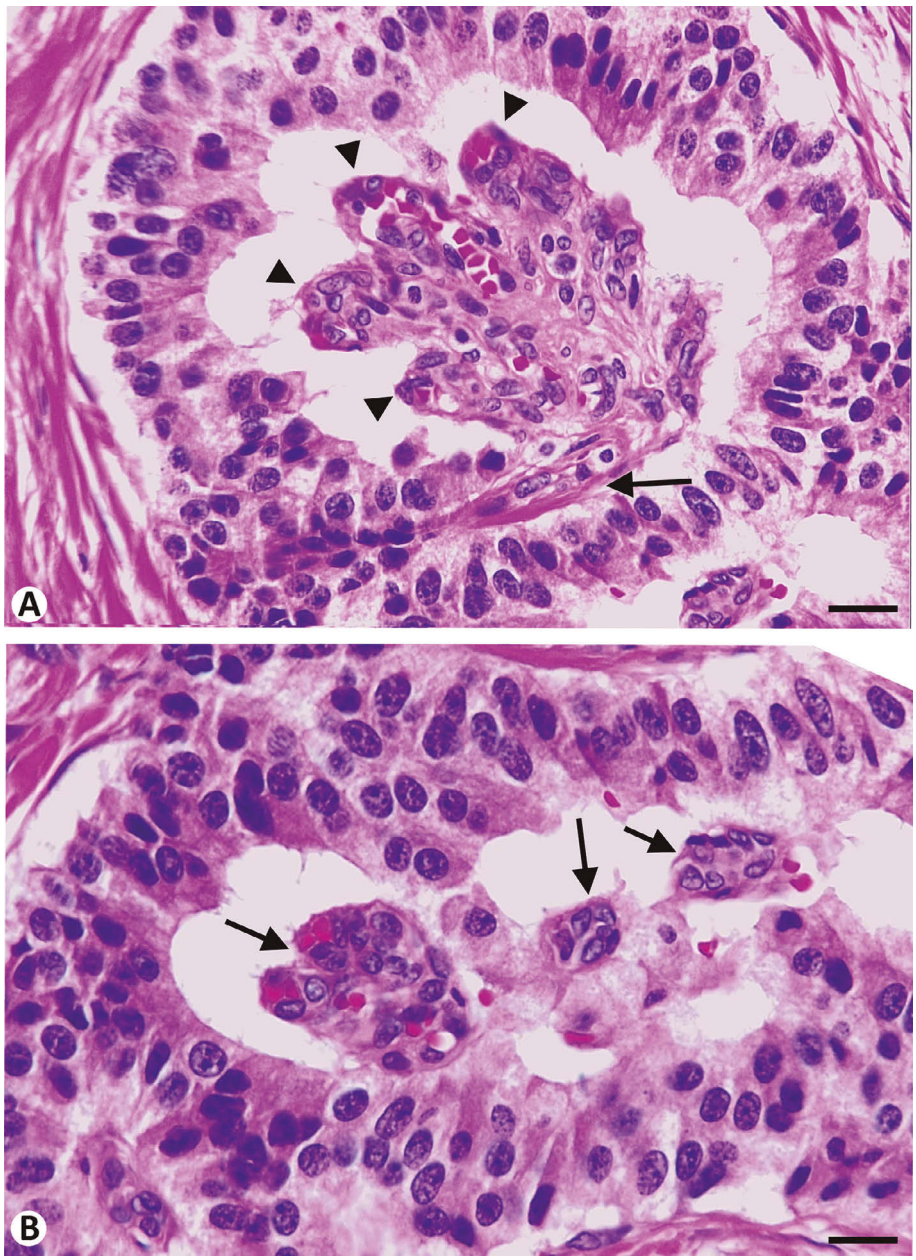

Fig. 4. A. A EVT in which several short branches (arrowheads) and a pedicle (arrow) are observed, with an oblique trajectory to the connective tissue. **B.** Several EVTs (arrows) tend to be associated in the convergent spaces of the neoplastic gyriform structures. In A and B, congestive blood vessels are seen. A, B: Hematoxylin and eosin staining. Scale bars: A, 20 µm; B, 15 µm.

Incidence of EVTs depending on the morphological pattern of PanNETs

Typical or modified EVTs were mainly observed in PanNETs in which the trabeculae and nests of neuroendocrine cells adopted a gyriform/winding ribbon pattern (in 84% of cases with this pattern), with EVTs occupying the central pseudoglandular space of the gyriform structures. EVTs were also seen in mixed patterns, in which the gyriform pattern was associated with others, mainly with the nested and cordonal (linear or undulate) patterns. Transitions between the trabecular gyriform and trabecular cordonal structures were frequently observed in cases with a mixed pattern. In these transitional areas, the EVT arrangement varied from central, in the gyriform structures, to laterally attached to the cords (Fig. 9), suggesting a progressive step from gyriform to cordonal (Fig. 9A-C). A correlation between the incidence of gyriform structures and that of EVTs was observed and became very evident in cases with a predominant gyriform pattern, the most frequent pattern in our cases. EVTs were uncommon (14.28% of cases) and poorly identifiable in PanNETs with solid patterns (Fig. 10A,B). Although EVTs can be present, their identification was more difficult when peliosis occurred in PanNETs (Fig. 10C). When venous

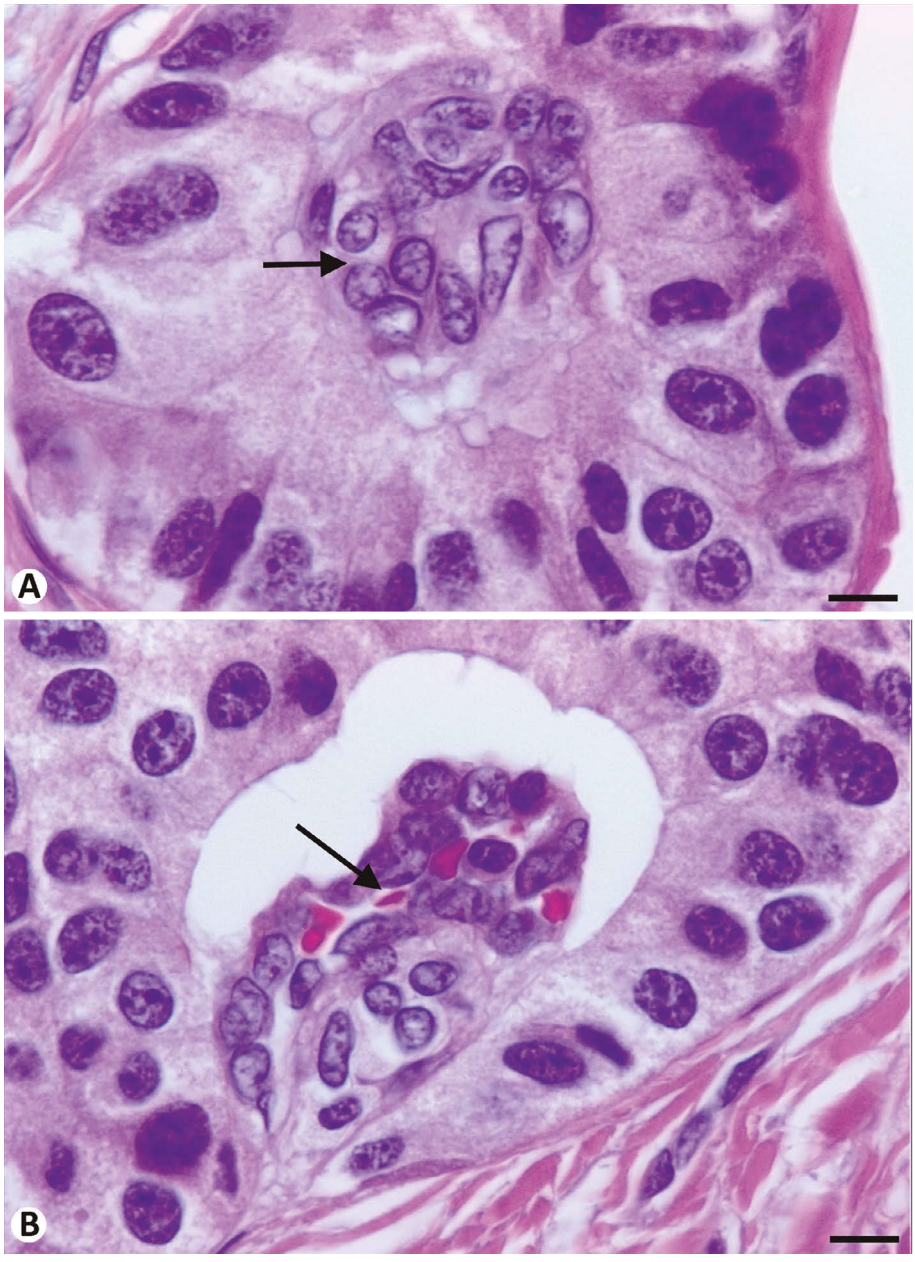

Fig. 5. A. Differences in the size and staining of the nuclei of EVT cells and those of the surrounding tumor neuroendocrine cells. Observe that the nuclei of the EVT cells (arrow) are smaller, less stained, and without the salt-and-pepper aspect of the surrounding neuroendocrine tumor cells. **B.** A EVT (arrow) in which the path of a blood vessel with intraluminal red blood cells is observed. A, B: Hematoxylin and eosin staining. Scale bars: A, 7 µm; B, 8 µm.

invasion manifested in PanNETs, the intraluminal surface of the invasive tumor appeared endothelialized and the tumor vascularization proceeded from this endothelialized surface and the perivenous microvasculature, without initial formation of EVTs (Fig. 10D,E,insert).

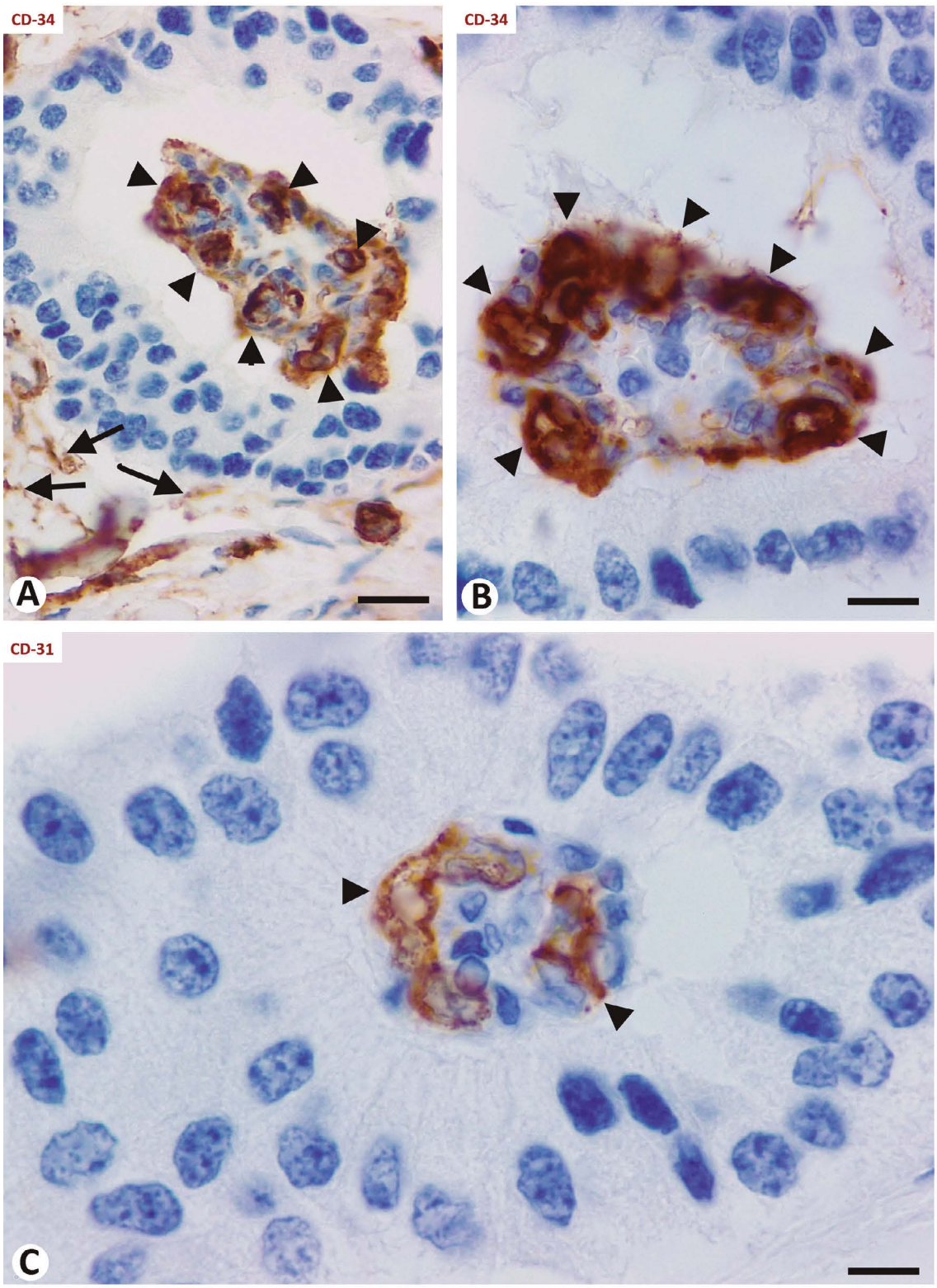

Fig. 6. Expression of CD34 (**A**, **B**, brown) and CD31 (**C**, brown) is observed in EVT endothelial cells and reveals a high number of blood vessels (arrowheads), including those with virtual lumens, non-identified by hematoxylin and eosin staining. Note CD34-positive stromal cells (arrows) in the connective tract around the gyriform neoplastic structure in A. A-C: Immunochemistry for CD34 (A, B) and CD31 (C). Hematoxylin counterstain. Scale bars: A, 20 µ; B, 15 µm; C, 10 µm.

Relationship between EVTs and connective tracts. Origin of EVT vessels and association with other dtructures

The relationship between EVTs and other stromal structural components was also evident in the neuroendocrine tumors in which trabeculae and cords of cuboidal or columnar cells adopt a gyriform/winding ribbon pattern. The relationship became more evident when the gyriform and winding ribbon structures were arranged independently or in groups (nests) between connective tracts of variable width and with different degrees of fibrosis. In these connective tracts, stromal cells expressing CD34, αSMA, and vimentin were an important component (Figs. 6A, 7A, 7B, 11). With these cell markers, mainly vimentin, the continuity of the pedicles of the EVTs with the connective tracts that surround the gyriform structures became even more evident (Fig. 11A). The proportion of stromal cells expressing either CD34 (CD34+ stromal cells/telocytes) or αSMA (myofibroblast-like cells) in the connective tracts varied depending on the case and the tumor area examined, ranging from balanced to practically only one of them. Likewise, the increase in αSMA-positive stromal cells was positively correlated with the degree of fibrosis.

EVT microvessels were observed originating from

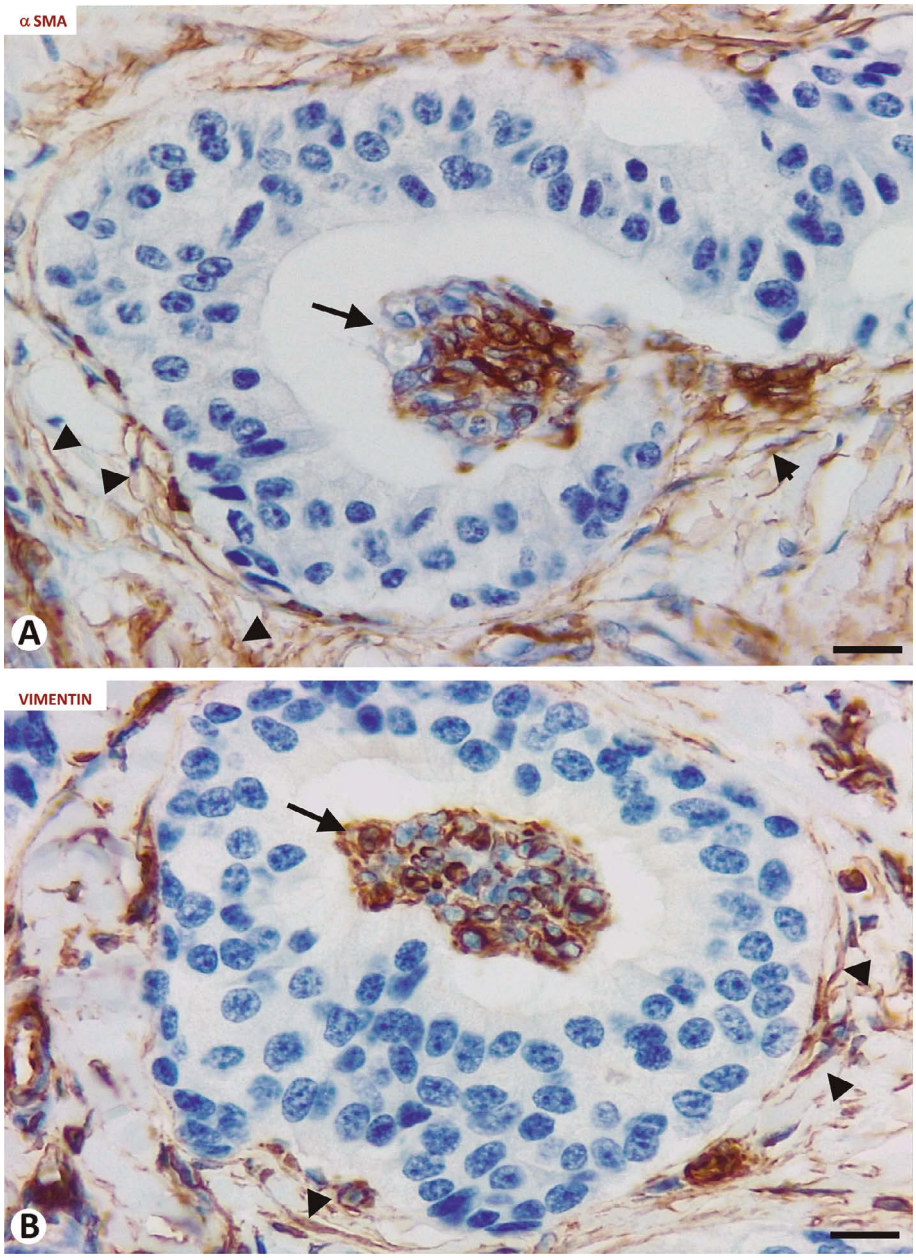

Fig. 7. A. Expression of αSMA (brown) in stromal and blood vessel mural cells in a EVT (arrow) and in the connective tract that surrounds a gyriform neoplastic structure (arrowheads). **B.** Endothelial, mural, and stromal cells expressing vimentin (brown) are observed in a central EVT (arrow) and the peripheral connective tract of a gyriform/pseudoglandular neoplastic structure (arrowheads). A: Immunochemistry for αSMA. B: Immunochemistry for vimentin. Hematoxylin counterstain. Scale bars: A, B, 15 μm.

small venules in the tracts of the connective tissue, above all when serial histological sections and immunochemistry procedures were used (Fig. 11B). The vessels in the connective tracts surrounded and adhered closely to the gyriform and winding ribbon structures, before penetrating and forming the vascular tufts within

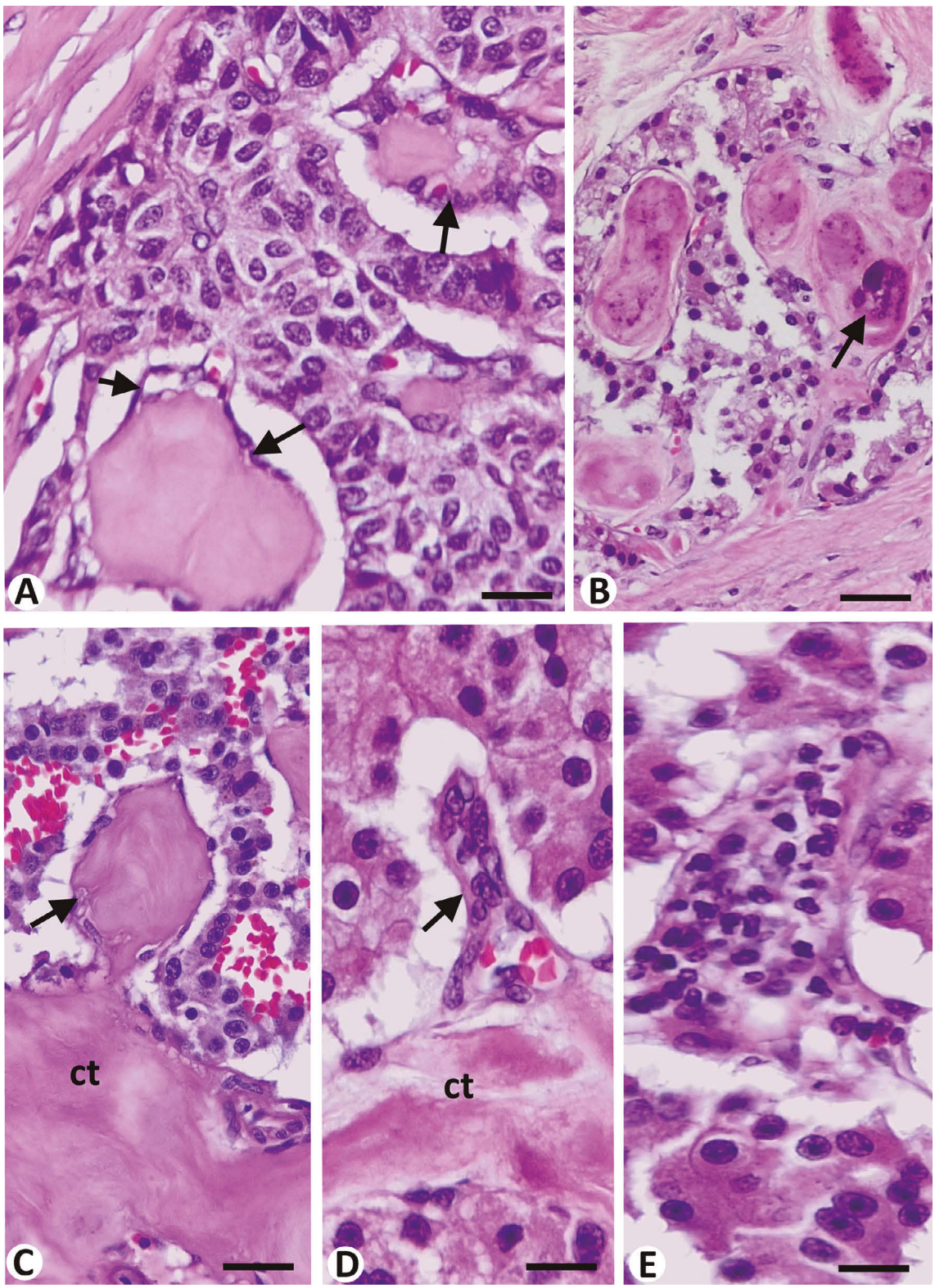

Fig. 8. Secondary changes in EVTs. **A, B.** EVTs increased in size and with hyaline changes (arrows). Note that the hyaline material pushes the microvessels toward their periphery, where they are compressed and form thin strips **(A, arrows)**. Calcification phenomena are observed in some EVTs **(B, arrow)**. **C, D.** EVTs with **(C, arrow)** and without **(D, arrow)** hyalinization are observed connecting with hyalinized peripheral connective tissue (ct) around gyriform structures. **E.** Infiltration of mononuclear inflammatory cells in an EVT. Hematoxylin and eosin staining. Scale bars: A, D, E, 20 µ; B, 40 µm; C, 30 µm.

(Fig. 8B).

In cases in which amyloid bodies were observed at the center of the gyriform structures, most of these bodies were arranged independently of the EVTs (insert in Fig. 11A) and only occasionally appeared associated with them.

Discussion

In this work, we report the presence of EVTs in PanNETs. EVTs are formed by 1) a vascular terminal area of the tuft, generally with a globular image (glomeruloid), separated by a space from surrounding tumor neuroendocrine cells (enclosing cells) and 2) a pedicle that joins the vascular terminal area to connective tracts around the surrounding tumor neuroendocrine cells. These structures may be considered the expression of a morphological sign, which we call a "vascular tuft sign". The glomeruloid appearance may go unnoticed because the microvessels may present virtual lumens, and the globular area adopts a highly cellular image upon hematoxylin and eosin staining, making it difficult to appreciate the vascular richness. In addition, the space generally formed between the tuft and the surrounding neuroendocrine cells may also disappear. In any case, the cells that make

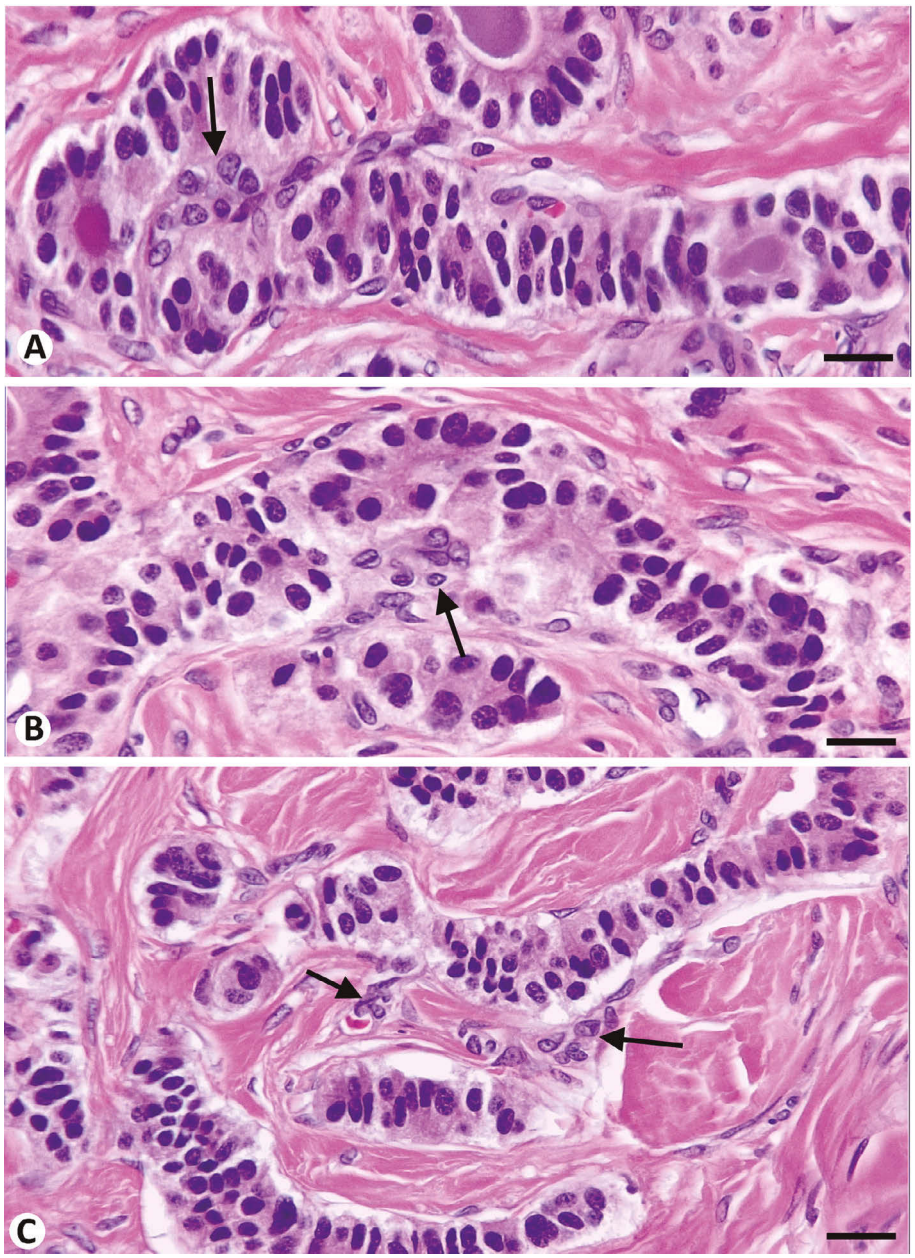

Fig. 9. EVT arrangement in transitional areas between trabecular gyriform and trabecular cordonal structures. Observe the EVT location in the center of the gyriform structure and laterally in the cordonal (arrows), which suggests a progressive step from gyriform to cordonal **(A-C)**. Hematoxylin and eosin staining. Scale bars: A, B, 20 µm; C, 25 µm.

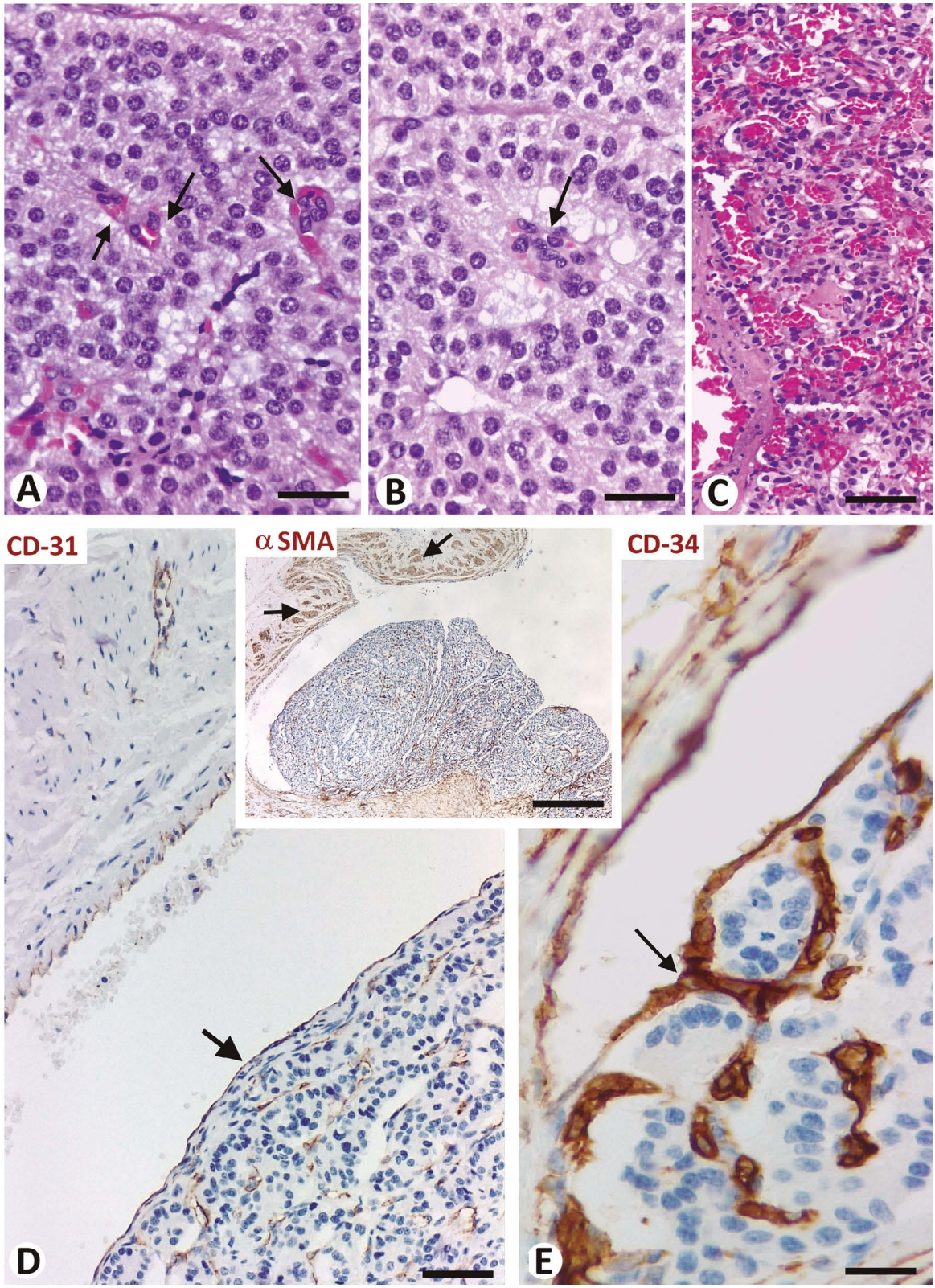

Fig. 10. A, B. EVTs in PanNETs with solid patterns. Note occasional poorly identifiable EVTs (arrows) in areas resembling a gyriform pattern. **C.** A region of PanNET with peliosis, in which EVT identification is difficult. **D, E.** PanNET venous invasion, in which the invasive tumor area is covered by CD31-positive (**D**, brown) and CD34-positive (**E**, brown) endothelial cells. Note an intratumoral microvessel originating from the endothelial surface (**E**, arrow). **Insert.** Characteristics and expression of αSMA in vascular smooth muscle cells (arrows) of the wall of the invaded vein. A-C: Hematoxylin and eosin staining. D: Immunochemistry for CD31. E: Immunochemistry for CD34. Insert: Immunochemistry for αSMA. C, D, and insert: Hematoxylin counterstain. Scale bars: A, B, 30 µ; C, D, 80 µ; E, 25 µm; Insert, 120 µm.

up the EVTs can be easily distinguished from the neuroendocrine tumor cells because their nuclei are smaller, paler, and lack the salt-and-pepper appearance typical of neuroendocrine tumor cells. Immunohistochemistry procedures highlighted the cluster of coiled microvessels in the glomeruloid area and their cell components: CD31- and CD34-positive endothelial cells, αSMA-positive pericytes, and perivascular CD34-positive stromal cells/telocytes.

The endocrine glands have a rich microvasculature, and neuroendocrine tumors are generally highly vascularized neoplasms, with vascularization levels up to 10 times greater than those found in carcinomas (Marion-Audibert et al., 2003; Carrasco et al., 2017;

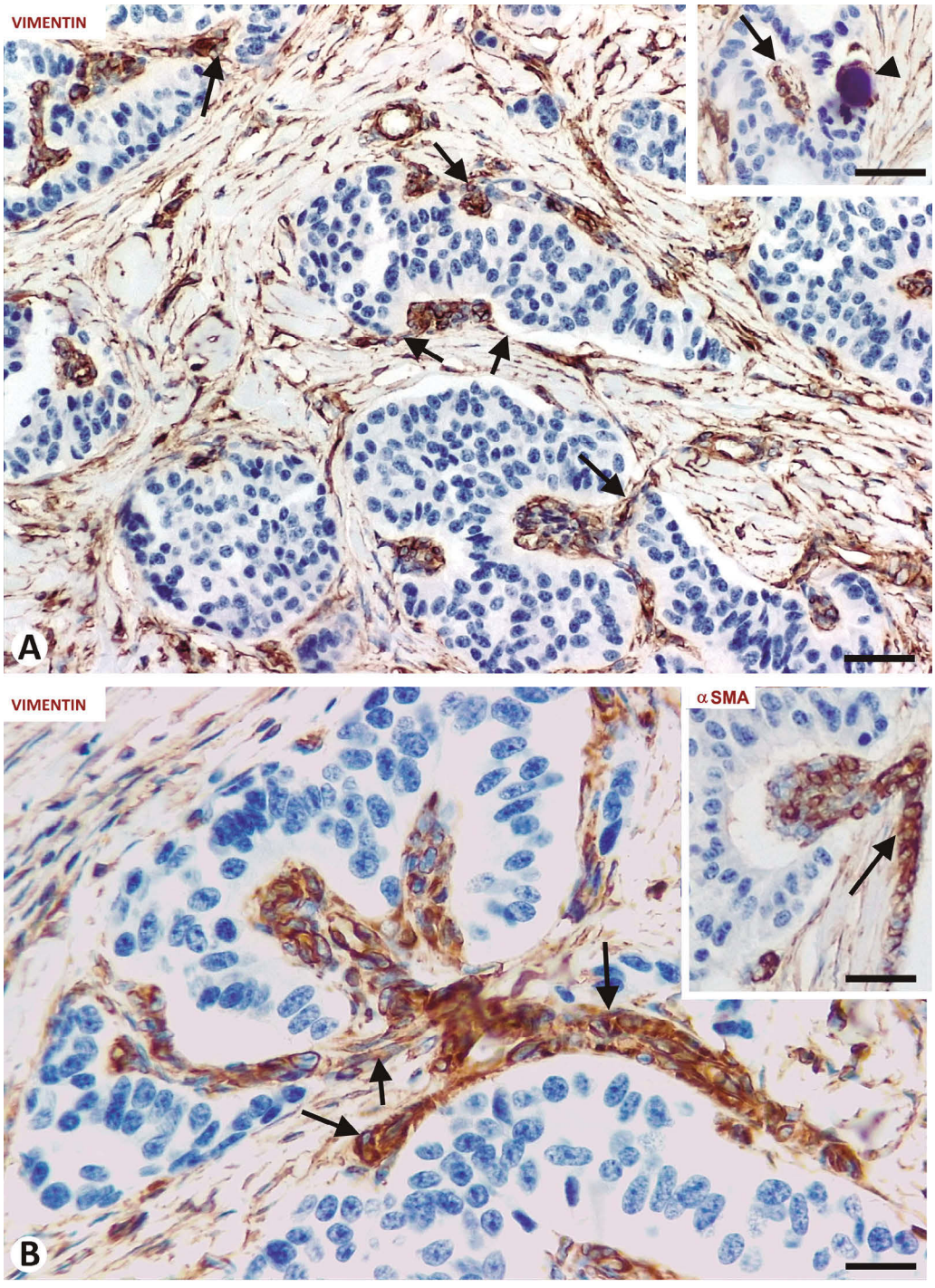

Fig. 11. A. Some pedicles of EVTs are seen in contact with the connective tracts surrounding the neoplastic gyriform structures (arrows). **Insert.** An EVT (arrow) and a psammoma body (arrowhead) in two different pseudoglandular spaces. **B, insert.** Microvessels in EVTs are observed originating from vessels in the connective tracts (arrows). Note that the vessels in the connective tracts are attached to the surface of the gyriform structures, following an arcuate path until the EVTs are formed through their pedicles. A, insert of A and B: Immunochemistry for vimentin. Hematoxylin counterstain. Insert of B: Immunochemistry for αSMA. Scale bars: A, 40 μm; B, 20 μm; insert of B, 30 μm.

Lauricella et al., 2022). Growth factors, including VEGF, PDGF, FGF, and angiopoietins, are involved in neuroendocrine tumors (Christofori et al., 1995; Terris et al.,1998; Katoh, 2003; Couvelard et al., 2005), in which the aberrant activation of the hypoxia-inducible factor pathway participates (Couvelard et al., 2005). Our observations lay the groundwork for further in-depth molecular studies on the mechanisms that specifically participate in the development and subsequent behavior of EVTs, which may be different in connective tracts. Indeed, secondary modifications in EVTs, such as fibrosis, hyalinization, edema, myxoid changes, and inflammatory infiltrates, may or may not coincide with those of the connective tracts.

The correlation between the incidence and various morphological patterns of PanNETs demonstrated that EVTs predominantly occur in the gyriform pattern, which was the most frequently observed in our study, especially when including the mixed variants where it is highly present. The higher incidence and expression of EVTs in the gyriform pattern and mixed variants (above all gyriform with nested or cordonal patterns) may be due to the arrangement of tumor trabeculae following a ribbon coil (winding ribbon pattern) around small vessels, which acquire the tufted image. As the small vessels are insulated by the surrounding trabeculae, staying connected by a pedicle to the connective tissue that in turn surrounds the tumor trabeculae, the characteristic image of the whole is obtained: EVTs occupy the central pseudoglandular space of tumor gyriform structures surrounded by connective tracts. Serial histological sections were useful for observing the tufts in gyriform structures that apparently lacked them and for following the transition of the tumor trabeculae from gyriform to cordonal (linear or undulate) in cases with this mixed pattern (gyriform and cordonal). Thus, as the connective tracts increase in size and the tumor trabeculae become cordonal, the EVTs lose their central position in the gyriform structures and become lateralized.

Psammoma bodies may be seen in the lumen of pseudoglandular structures in some cases of PanNETs (Greider et al., 1984; Garbrecht et al., 2008; Samad et al., 2014; Olivas and Antic, 2019). These bodies are usually observed in somatostatin-secreting neuroendocrine tumors (Garbrecht et al., 2008). In our cases, in which EVTs and psammoma bodies were present, they rarely appeared associated with each other, although they were intraluminal. This rare association suggests that EVTs play a small role in the development of psammoma bodies.

The tumor microenvironment in neuroendocrine tumors has been extensively considered (Laskaratos et al., 2017; Cives et al., 2019; Takkenkamp et al., 2020; Lai et al., 2024), and particular attention has been paid to pancreatic stellate cells, especially their implications in pancreatic fibrosis (Bachem et al., 1998; Apte et al., 1999; Xue et al., 2018; Chang et al., 2023). However, the presence of CD34-positive stromal cells/telocytes in the stroma of PanNETs is largely absent in the literature, despite the descriptions of telocytes as an important stromal component under normal conditions of the pancreas (Nicolescu and Popescu, 2012; Zhang et al., 2016; Gandahi et al., 2020). It has been demonstrated that *in situ* native CD34-positive stromal cells/telocytes have progenitor capacity, are a source of αSMA-positive myofibroblast cells, and may be activated with and without myofibroblast transformation (Díaz-Flores et al., 2015a,b, 2021). The fact that in our observations, stromal cells in PanNETs could express either CD34 or αSMA in different proportions, depending on the case and the tumor region examined, can be related to this capacity of CD34-positive stromal cells/telocytes and therefore to their participation in pancreatic fibrosis associated with PanNETs. Future studies in this regard would be of interest.

Venous invasion by PanNETs has been widely studied, including intra- and extra-tumoral macrovascular invasion (Bok et al., 1984; Schmid et al., 2005; Balachandran et al., 2012; Addeo et al., 2019; Shi et al.,2023). The absence of EVTs in initial groups of tumoral cells located within veins may be due to the origin of their microvasculature: endothelialized intraluminal tumor surface or adventitial microcirculation. Venous invasion in PanNETs resembles that of angioinvasive follicular thyroid carcinoma, in which we have observed findings that support a piecemeal mechanism related to intussusceptive angiogenesis (Díaz-Flores et al., 2017). By this mechanism, venous endothelial cells grow out of the vessel and form loops, encircling groups of tumoral cells that are incorporated (transported) into the vein lumen. Thus, the tumor cells are surrounded by endothelial cells from the beginning, which could explain why the tumor progresses through the venous route, reaching the form of macrovascular invasion.

In conclusion, we contribute a morphological "vascular tuft sign" in PanNETs, mainly present in cases with a predominant trabecular and nested gyriform pattern. The "vascular tuft sign" is defined by the presence of vascular tufts enclosed by the trabeculae of tumor neuroendocrine cells, which are in turn surrounded by connective tissue tracts (EVTs). Fibrosis, and degenerative and inflammatory findings in EVTs may or may not coincide with those in connective tracts. Future studies are mainly required on the mechanisms of EVT formation and the behavior of their perivascular stromal cells when compared with those of connective tracts. Also of interest is the exploration of EVTs in neuroendocrine tumors of other organs.

Acknowledgements. The authors would like to thank Kim Eddy for the English revision.

Conflicts of Interest. The authors declare no conflict of interest.

References

Addeo P., d'Alessandro A., Averous G., Imperiale A., Faitot F., Goichot B. and Bachellier P. (2019). Macrovascular venous invasion of

pancreatic neuroendocrine tumours: impact on surgical outcomes and survival. HPB (Oxford). 21, 653-661.

Apte M.V., Haber P.S., Darby S.J., Rodgers S.C., McCaughan G.W., Korsten M.A., Pirola R.C. and Wilson J.S. (1999). Pancreatic stellate cells are activated by proinflammatory cytokines: implications for pancreatic fibrogenesis. Gut 44, 534-541.

Bachem M.G., Schneider E., Gross H., Weidenbach H., Schmid R.M., Menke A., Siech M., Beger H., Grünert A. and Adler G. (1998). Identification, culture, and characterization of pancreatic stellate cells in rats and humans. Gastroenterology 115, 421-432.

Balachandran A., Tamm E.P., Bhosale P.R., Katz M.H., Fleming J.B., Yao J.C. and Charnsangavej C. (2012). Venous tumor thrombus in nonfunctional pancreatic neuroendocrine tumors. Am. J. Roentgenol. 199, 602-608.

Bok E.J., Cho K.J., Williams D.M., Brady T.M., Weiss C.A. and Forrest M.E. (1984). Venous involvement in islet cell tumors of the pancreas. Am. J. Roentgenol. 142, 319-322.

Carrasco P., Zuazo-Gaztelu I. and Casanovas O. (2017). Sprouting strategies and dead ends in anti-angiogenic targeting of NETs. J. Mol. Endocrinol. 59, R77-R91.

Chang M., Chen W., Xia R., Peng Y., Niu P. and Fan H. (2023). Pancreatic stellate cells and the targeted therapeutic strategies in chronic pancreatitis. Molecules 28, 5586.

Chmiel P., Rychcik-Pazyrska P. and Stec R. (2023). Defining tumor microenvironment as a possible target for effective GEP-NENs immunotherapy-A systematic review. Cancers 15, 5232.

Christofori G., Naik P. and Hanahan D. (1995). Vascular endothelial growth factor and its receptors, flt-1 and flk-1, are expressed in normal pancreatic islets and throughout islet cell tumorigenesis. Mol. Endocrinol. 9, 1760-1770.

Cives M., Pelle E., Quaresmini D., Rizzo F.M., Tucci M. and Silvestris F. (2019). The tumor microenvironment in neuroendocrine tumors: Biology and therapeutic implications. Neuroendocrinology 109, 83-99.

Couvelard A., O'Toole D., Turley H., Leek R., Sauvanet A., Degott C., Ruszniewski P., Belghiti J., Harris A. L., Gatter K. and Pezzella F. (2005). Microvascular density and hypoxia-inducible factor pathway in pancreatic endocrine tumours: negative correlation of microvascular density and VEGF expression with tumour progression. Br. J. Cancer 92, 94-101.

Dasari A., Shen C., Halperin D., Zhao B., Zhou S., Xu Y., Shih T. and Yao J. C. (2017). Trends in the incidence, prevalence, and survival outcomes in patients with neuroendocrine tumors in the United States. JAMA Oncol. 3, 1335-1342.

Díaz-Flores L., Gutiérrez R., Lizartza K., González-Goméz M., García M.P., Sáez F. J., Díaz-Flores L. Jr. and Madrid J.F. (2015a). Behavior of *in situ* human native adipose tissue CD34+ stromal/progenitor cells during different stages of repair. Tissue-resident CD34+ stromal cells as a source of myofibroblasts. Anat. Rec. 298, 917-930.

Díaz-Flores L., Gutiérrez R., García M.P., González M., Sáez F.J., Aparicio F., Díaz-Flores L. Jr. and Madrid J.F. (2015b). Human resident CD34+ stromal cells/telocytes have progenitor capacity and are a source of αSMA+ cells during repair. Histol. Histopathol. 30, 615-627.

Díaz-Flores L., Gutiérrez R., García-Suárez M. P., Sáez F. J., Gutiérrez E., Valladares F., Carrasco J.L., Díaz-Flores L. Jr. and Madrid J.F. (2017). Morphofunctional basis of the different types of angiogenesis and formation of postnatal angiogenesis-related secondary structures. Histol. Histopathol. 32, 1239-1279.

Díaz-Flores L., Gutiérrez R., García M.P., González-Gómez M., Sáez F.J., Díaz-Flores L. Jr., Carrasco J.L. and Madrid J.F. (2018). Sinusoidal hemangioma and intravascular papillary endothelial hyperplasia: Interrelated processes that share a histogenetic piecemeal angiogenic mechanism. Acta Histochem. 120, 255-262.

Díaz-Flores L., Gutiérrez R., González-Gómez M., García M.P., Díaz-Flores L. Jr, Carrasco J.L. and Martín-Vasallo P. (2021). CD34+ stromal cells/Telocytes as a source of cancer-associated fibroblasts (CAFs) in invasive lobular carcinoma of the breast. Int. J. Mol. Sci. 22, 3686.

Díaz-Flores L., Gutiérrez R., González-Gómez M., García M.P., Palmas M., Carrasco J.L., Madrid J.F. and Díaz-Flores L. Jr. (2023). Delimiting CD34+ Stromal Cells/Telocytes are resident mesenchymal cells that participate in neovessel formation in skin Kaposi sarcoma. Int. J. Mol. Sci. 24, 3793.

Falconi M., Bartsch D.K., Eriksson B., Klöppel G., Lopes J.M., O'Connor J.M., Salazar R., Taal B.G., Vullierme M.P., O'Toole D. and Barcelona Consensus Conference participants. (2012). ENETS Consensus guidelines for the management of patients with digestive neuroendocrine neoplasms of the digestive system: well-differentiated pancreatic non-functioning tumors. Neuroendocrinology 95, 120-134.

Gandahi N.S., Ding B., Shi Y., Bai X., Gandahi J.A., Vistro W.A., Chen Q. and Yang P. (2020). Identification of telocytes in the pancreas of Turtles-A role in cellular communication. Int. J. Mol. Sci. 21, 2057.

Garbrecht N., Anlauf M., Schmitt A., Henopp T., Sipos B., Raffel A., Eisenberger C.F., Knoefel W.T., Pavel M., Fottner C., Musholt T.J., Rinke A., Arnold R., Berndt U., Plöckinger U., Wiedenmann B., Moch H., Heitz P.U., Komminoth P., Perren A. and Klöppel G. (2008). Somatostatin-producing neuroendocrine tumors of the duodenum and pancreas: incidence, types, biological behavior, association with inherited syndromes, and functional activity. End. Rel. Cancer. 15, 229-241.

Greider M.H., DeSchryver-Kecskemeti K. and Kraus F.T. (1984). Psammoma bodies in endocrine tumors of the gastroentero-pancreatic axis: a rather common occurrence. Sem. Diag. Pathol. 1, 19-29.

Kasajima A. and Klöppel G. (2020). Neuroendocrine neoplasms of lung, pancreas and gut: a morphology-based comparison. End. Rel. Cancer 27, R417-R432.

Katoh R. (2003). Angiogenesis in endocrine glands: special reference to the expression of vascular endothelial growth factor. Microsc. Res. Tech. 60, 181-185.

Kim J.Y., Hong S.M. and Ro J.Y. (2017). Recent updates on grading and classification of neuroendocrine tumors. Ann. Diag. Pathol. 29, 11-16.

Klimstra D.S., Modlin I.R., Coppola D., Lloyd R.V. and Suster S. (2010). The pathologic classification of neuroendocrine tumors: a review of nomenclature, grading, and staging systems. Pancreas 39, 707-712.

Konukiewitz B., Schlitter A.M., Jesinghaus M., Pfister D., Steiger K., Segler A., Agaimy A., Sipos B., Zamboni G., Weichert W., Esposito I., Pfarr N. and Klöppel, G. (2017). Somatostatin receptor expression related to TP53 and RB1 alterations in pancreatic and extrapancreatic neuroendocrine neoplasms with a Ki67-index above 20. Mod. Pathol. 30, 587-598.

Konukiewitz B., von Hornstein M., Jesinghaus M., Steiger K., Weichert W., Detlefsen S., Kasajima A. and Klöppel G. (2020). Pancreatic neuroendocrine tumors with somatostatin expression and

paraganglioma-like features. Human Pathol. 102, 79-87.

Lafaro K.J. and Melstrom L.G. (2019). The paradoxical web of pancreatic cancer tumor Microenvironment. Am. J. Pathol. 189, 44-57.

Lai T.Y., Chiang T.C., Lee C.Y., Kuo T.C., Wu C.H., Chen Y.I., Hu C.M., Maskey M., Tang S.C., Jeng Y.M., Tien Y.W., Lee E.Y.P. and Lee W.H. (2024). Unraveling the impact of cancer-associated fibroblasts on hypovascular pancreatic neuroendocrine tumors. Br. J. Cancer 130, 1096-1108.

Laskaratos F.M., Rombouts K., Caplin M., Toumpanakis C., Thirlwell C. and Mandair D. (2017). Neuroendocrine tumors and fibrosis: An unsolved mystery? Cancer 123, 4770-4790.

Lauricella E., Mandriani B., Cavallo F., Pezzicoli G., Chaoul N., Porta C. and Cives, M. (2022). Angiogenesis in NENs, with a focus on gastroenteropancreatic NENs: from biology to current and future therapeutic implications. Front. Oncol. 12, 957068.

Liu Q. and Polydorides A. D. (2020). Diagnosis and prognostic significance of extramural venous invasion in neuroendocrine tumors of the small intestine. Mod. Pathol. 33, 2318-2329.

Marion-Audibert A.M., Barel C., Gouysse G., Dumortier J., Pilleul F., Pourreyron C., Hervieu V., Poncet G., Lombard-Bohas C., Chayvialle J.A., Partensky C. and Scoazec J.Y. (2003). Low microvessel density is an unfavorable histoprognostic factor in pancreatic endocrine tumors. Gastroenterology 125, 1094-1104.

McCall C.M., Shi C., Klein A.P., Konukiewitz B., Edil B.H., Ellison T.A., Wolfgang C.L., Schulick R.D., Klöppel G. and Hruban R.H. (2012). Serotonin expression in pancreatic neuroendocrine tumors correlates with a trabecular histologic pattern and large duct involvement. Human Pathol. 43, 1169-1176.

Nicolescu M.I. and Popescu L.M. (2012). Telocytes in the interstitium of human exocrine pancreas: ultrastructural evidence. Pancreas 41, 949-956.

Norton J.A., Harris E.J., Chen Y., Visser B.C., Poultsides G.A., Kunz P.C., Fisher G.A. and Jensen R.T. (2011). Pancreatic endocrine tumors with major vascular abutment, involvement, or encasement and indication for resection. Arch. Surg. (Chicago). 146, 724-732.

Olivas A. and Antic T. (2019).The presence of psammoma bodies in a gastroentero-pancreatic neuroendocrine tumor should raise the suspicion for a diagnosis of somatostatinoma in cytology specimens. J. Am. Soc. Cytopathol. 8, S19-S20.

Rindi G., Mete O., Uccella S., Basturk O., La Rosa S., Brosens L.A.A., Ezzat S., de Herder W.W., Klimstra D.S., Papotti M. and Asa S.L. (2022). Overview of the 2022 WHO Classification of Neuroendocrine Neoplasms. Endocr. Pathol. 33, 115-154.

Rossi R.E. and Massironi S. (2022). The increasing incidence of neuroendocrine neoplasms worldwide: Current knowledge and open issues. J. Clin. Med. 11, 3794.

Samad A., Attam R., Jessurun J. and Pambuccian S.E. (2014). Psammoma bodies and abundant stromal amyloid in an endoscopic ultrasound guided fine needle aspirate (EUS-FNA) of a pancreatic neuroendocrine tumor: a potential pitfall. Diagn. Cytopathol. 42, 766-771.

Schmid K., Birner P., Gravenhorst V., End A. and Geleff S. (2005). Prognostic value of lymphatic and blood vessel invasion in neuroendocrine tumors of the lung. Am. J. Pathol. 29, 324-328.

Shi C., Chen W., Davis R. and Morse M.A. (2023). Venous invasion in pancreatic neuroendocrine tumors is independently associated with disease-free survival and overall survival. Am. J. Surg. Pathol. 47, 678-685.

Takkenkamp T.J., Jalving M., Hoogwater F.J.H. and Walenkamp A.M.E. (2020). The immune tumour microenvironment of neuroendocrine tumours and its implications for immune checkpoint inhibitors. Endocr. Relat. Cancer 27, R329-R343.

Terris B., Scoazec J.Y., Rubbia L., Bregeaud L., Pepper M.S., Ruszniewski P., Belghiti J., Fléjou J. and Degott C. (1998). Expression of vascular endothelial growth factor in digestive neuroendocrine tumours. Histopathology 32, 133-138.

Xu Z., Wang L., Dai S., Chen M., Li F., Sun J. and Luo F. (2021). Epidemiologic trends of and factors associated with overall survival for patients with gastroenteropancreatic neuroendocrine tumors in the United States. JAMA 4, e2124750.

Xue R., Jia K., Wang J., Yang L., Wang Y., Gao L. and Hao J. (2018). A rising star in pancreatic diseases: Pancreatic stellate cells. Front. Physiol. 9, 754.

Xue Y., Reid M.D., Pehlivanoglu B., Obeng R.C., Jiang H., Memis B., Lui S.K., Sarmiento J., Kooby D., Maithel S.K., El-Rayes B., Basturk O. and Adsay V. (2020). Morphologic variants of pancreatic neuroendocrine tumors: Clinicopathologic analysis and prognostic stratification. Endocr. Pathol. 31, 239-253.

Yang M., Zeng L., Ke N.W., Tan C.L., Tian B.L., Liu X.B., Xiang B. and Zhang Y. (2020). World Health Organization grading classification for pancreatic neuroendocrine neoplasms: a comprehensive analysis from a large Chinese institution. BMC Cancer 20, 906.

Zhang H., Yu P., Zhong S., Ge T., Peng S., Guo X. and Zhou Z. (2016). Telocytes in pancreas of the Chinese giant salamander (*Andrias davidianus*). J. Cell Mol. Med. 20, 2215-2219.

Accepted June 27, 2024